

Article

Narrow Bandwidth Top-Emitting OLEDs Designed for Rhodamine 6G Excitation in Biological Sensing Applications

Matthias Jahnelt^{1,*}, Beatrice Beyer¹, Michael Thomschke¹, Karsten Fehse¹, Felix Krujatz² and Karl Leo³

¹ Fraunhofer Institute for Organic Electronics, Electron Beam and Plasma Technology FEP, Maria-Reiche-Str. 02, Dresden 01199, Germany;

E-Mails: beatrice.beyer@comedd.fraunhofer.de (B.B.);

michael.thomschke@comedd.fraunhofer.de (M.T.); karsten.fehse@comedd.fraunhofer.de (K.F.)

² Institute of Food Technology and Bioprocess Engineering, Bergstraße, Dresden 01069, Germany;

E-Mail: felix.krujatz@tu-dresden.de

³ Institut für Angewandte Photophysik, Technische Universität Dresden, Dresden 01062, Germany;

E-Mail: karl.leo@iapp.de

* Author to whom correspondence should be addressed; E-Mail: matthias.jahnelt@fep.fraunhofer.de; Tel.: +49-351-8823-206; Fax: +49-351-8823-394.

Academic Editor: Mohan Jacob

Received: 2 September 2015 / Accepted: 10 November 2015 / Published: 25 November 2015

Abstract: Organic light emitting diodes (OLED) are promising candidates offering in optical sensor applications to detect different gas compositions and excitable optical marker groups in chemical and biological processes. They enable attractive solutions for monitoring the gas phase composition of e.g., dissolved molecular oxygen (O₂) species in bio reactors or excitation of fluorescent markers. In this work, we investigate different OLED devices for biomedical applications to excite the fluorescent dye rhodamine 6G (R6G). The OLED devices are built in top emission geometry comprising a distributed Bragg reflector (DBR) acting as optical mirror. The OLED is optimized to provide a very narrow emission characteristic to excite the R6G at 530 nm wavelength and enabling the possibility to minimize the optical crosstalk between the OLED electroluminescence and the fluorescence of R6G. The DBR includes a thin film encapsulation and enables the narrowing of the spectral emission band depending on the number of DBR pairs. The comparison between optical simulation data and experimental results exhibits good agreement and proves process stability.

Keywords: OLED; sensoric; DBR; biochemical sensor; Rhadamin6G; narrow emission; lab on chip

1. Introduction

The technology of organic light emitting diode (OLED) based sensors is a new and emerging field in research and development that potentially enables attractive solutions for monitoring different gas phase compositions [1,2], to detect dissolved molecular oxygen (O₂) species [2] or as excitation light source for fluorescent or phosphorescent markers in biological systems and chemical processes [2]. The OLED in photoluminescence (PL) based sensors operates commonly in pulse mode and enables by excitation the monitoring of any effects on the PL intensity induced by an analyte and also on its PL decay time. Besides PL based sensing in microscopy [3,4], fluorescence studies of cells [5,6] and forensic trace evidence [7] are well established methods in biological and chemical studies and offer extensive possibilities to observe cell growth, metabolism behavior and toxicological effects. However, a remaining challenge is to detect changes in the PL intensity and that the excitation and emission spectrum for bio or chemical markers need to be sufficiently separated. In order to reduce the spectrally overlapping light fractions, two approaches are possible: (i) either expanding the Stokes-shift of the marker molecule as much as possible by choosing optimum emitting and excitable analytes or (ii) by applying additional optical components for the excitation source (e.g., by distributed Bragg reflectors (DBRs)) or optical filter on the photodiode (band-pass, long-pass filters). Conventional OLEDs, which are applied in combination with such optical filters, are usually based on a bottom emission architecture, where the emitted light passes through the transparent electrode and substrate [8,9]. In the past, optical mirrors such as DBRs have only been used to improve the light extraction for increase of the light outcoupling efficiency [10–13] or to realize optical lasing [14]. However, there is also the possibility to integrate OLED and filter in sensor technology in very compact designs as well as nearly unlimited shapes and sizes of homogeneous emission area. Based on the emission and excitation profile, several biological and chemical processes can be detected by fluorescent or phosphorescent dye molecules. Rhodamine 6G (R6G) is a derivate of the xanthene class and a highly fluorescent dye. R6G features a high quantum yield of e.g., 95% in ethanol or water and shows an absorption peak at 530 nm in ethanol. It is often used as a water soluble tracer dye to determine the rate, transport or flow direction in bio-medical sensing applications. Moreover, the R6G dye is extensively used in biotechnology applications such as fluorescence microscopy [3], fluorescence correlation spectroscopy [4], flow cytometry [8] and enzyme-linked immunosorbent assays [15]. Optical sensors that are based on the stimulation of oxygen-sensitive dyes or derivatives of the xanthene group like R6G dyes are still in the focus of continuous effort to enhance the sensors accuracy, reliability, detection limit, operational lifetime or to reduce their cost and size [2]. For these requirements, organic sensors can offer a wide range of advantages such as low cost production, versatility, applicability, disposability, flexibility and a compact size of the whole architecture [2,11], hence being very attractive for medical [16], biological [17–20] environmental [21,22] and industrial applications [17].

In this study, we investigate three OLED device architectures in top emission geometry adjusted to the needs of R6G. The OLEDs are fabricated on a 200 mm silicon wafer substrate with a variation of dielectric DBR mirrors to achieve a defined and narrow green OLED emission spectra to efficiently excite the analyte R6G for PL based sensing. The green OLEDs are combined with DBR mirror and include a thin-film encapsulation. With this architecture, it is possible to provide a sufficiently narrow OLED emission to excite R6G and to be separated from the resulting R6G emission itself. The DBR on top of the OLED is designed to stimulate the excitation maximum of R6G at 530 nm and to have a cutoff at 550 nm for minimum overlap with fluorescence of the R6G. We discuss the challenges to fabricate the DBR on top of the OLED and compare the results to a reference OLED without any mirror. Additionally, we investigate the current density—voltage characteristics (j - V), the luminance (L), the radiance (R) and external quantum efficiency (EQE) and the light emission spectra regarding loss channels and band shifts. Furthermore, the results are compared with optical simulation data taking the optical properties of DBR mirrors into account.

2. Results and Discussion

In Figure 1, plot (a) and (b) exhibit the J - V and L - V characteristics, respectively. The data of the reference device (without any DBR) is represented by the black rectangles and shows a steep rise between 2 V and 3 V and a moderate increase towards 5.45 V at 50 mA/cm². For the reference device, the luminance (see plot b) reaches approximately 100 cd/m² at 3.10 V and rises up to about 8365 cd/m² at 5.61 V. Our reference device shows comparable results in performance to the manuscript of Peng [23] for OLED devices with a fluorescent green top emission architecture. In comparison to the voltage V at 50 mA/cm², we see a fundamental shift of the operation voltage from 5.45 V for the reference to maximum of 9.08 V with increasing DBR pair number, see Table 1. The OLED device with the highest number of DBR pairs ($n = 6$ pairs, green upside-down triangle) shows the highest difference in J - V and L - V characteristics to the reference with no DBR-layer. The voltage at 10,000 cd/m² shows the same behavior and increases with the number of DBR-layers. We notice the difference between the voltage at 50 mA/cm² to the voltage at 10,000 cd/m² (see Table 1). Further, the voltage increases in different amounts with respect to the number of applied DBR pairs. We see a large difference from 0 to two pairs and a slight difference from four to six pairs. This difference illustrates the declining efficiency in Figure 1 with increasing number of DBR-layers. The device shows less current at a given voltage and subsequently less luminance which depends on decreased current densities for the devices with DBRs (Figure 1a). These changes of the OLED device characteristic is caused by compressive or tensile stress [24], which is most likely induced by the oxide DBR layers on the devices or a temperature effect [25] to the OLED materials. A typical OLED deposition process is limited to maximum substrate temperature of 100 °C, but TiO₂ cause a temperature increase of the substrate during electronic-beam deposition of up to 120 °C, respectively. Such high deposition temperatures can cause morphology changes within the OLED layer, as well as diffusion of materials to neighboring layers and degradation of molecules. The luminous efficiency is significantly affected by the drop of the luminance at the same current density. We considered the luminance L at 50 mA/cm² and compared it to simulation results. As expected, a lower efficiency at equal current density is observed. This is partly due to the losses within the device and is essential to the optical properties of the components. In comparison to the simulation of the maximum luminance

relative to our measurements, we see that the simulated luminance behaves as similar as in the experiment. The OLED luminance with 0 pairs and the current density of 50 mA/cm^2 is 8365 cd/m^2 and rises as expected to 8685 cd/m^2 for the OLED with two DBR pairs. Considering the luminance of the OLED with four and six DBR pairs, we see a significant loss in the efficiency compared to the reference. Accordingly to the differences in voltage and peak efficiency we see more pronounced losses for lower luminance values between the reference OLED and the devices with DBR mirror. The current efficiency of OLEDs increase with current density up to the point of optimum recombination properties within the emitting layer [26]. In contrast to the simulated and measured luminance we see a difference between six and four pairs of DBR. This difference is based on changed recombination properties and a variation of layer thickness in comparison to the ideal and fixed layer thickness in simulation. The results show that the addition of the DBR-layer onto the OLED device causes a shift of the maximum current efficiency towards higher current densities and luminance. As a consequence, Figure 1c exhibits the drop of efficiency of approximately 56% at 1000 cd/m^2 for the device with maximum numbers of DBR compared to the reference device. When comparing the OLED luminance and current efficiency with the radiometric properties (Figure 1e) and external quantum efficiency EQE (Figure 1f), we see the same behavior. The radiance of the OLEDs decreases with increasing number of DBR pairs. In comparison to the voltage at $10 \text{ W}/(\text{m}^2 \times \text{sr})$, we see the shift from 5.0 V (reference device) to 9.45 V (OLED device with six pairs of DBR), which resulted in the most significant shift of radiance and current density compared to the device with less DBR pairs, while a significant loss in the EQE is observed between the device with four and six DBR pairs. Figure 1f exhibits a decreasing of EQE at 8 V from 4.2% for reference to 2.1% for device with six pair DBR. Regarding the differences in voltage and EQE we see more pronounced losses for lower radiance values between the reference OLED and the devices with DBR mirror. We attribute these changes in the electro-optical characteristics to the adoption of dielectric mirrors on top of the OLED and their thermal or mechanical influence on the organic layer during the deposition, since the OLED layer thicknesses show no changes in their SEM cross sections.

Table 1. Comparison of measured voltage, (V at 50 mA/cm^2 and V at 10 kcd/m^2) and measured luminance (L at 50 mA/cm^2) with the simulated luminance $L_{\text{simulated}}$ in percent normalized to reference organic light emitting diodes (OLED) depending on the distributed Bragg reflector (DBR) structure.

Pairs	V at 50 mA/cm^2	V at $10,000 \text{ cd/m}^2$	L at 50 mA/cm^2	L_{measured}	$L_{\text{simulated}}$	EQE at 8 V
N	(V)	(V)	(cd/m^2)	(%)	(%)	(%)
0	5.45	5.61	8365	100	100	4.2
2	8.43	8.58	8685	104	110	4.6
4	8.52	9.12	5980	71	79	3.0
6	9.08	10.12	4104	49	43	2.1

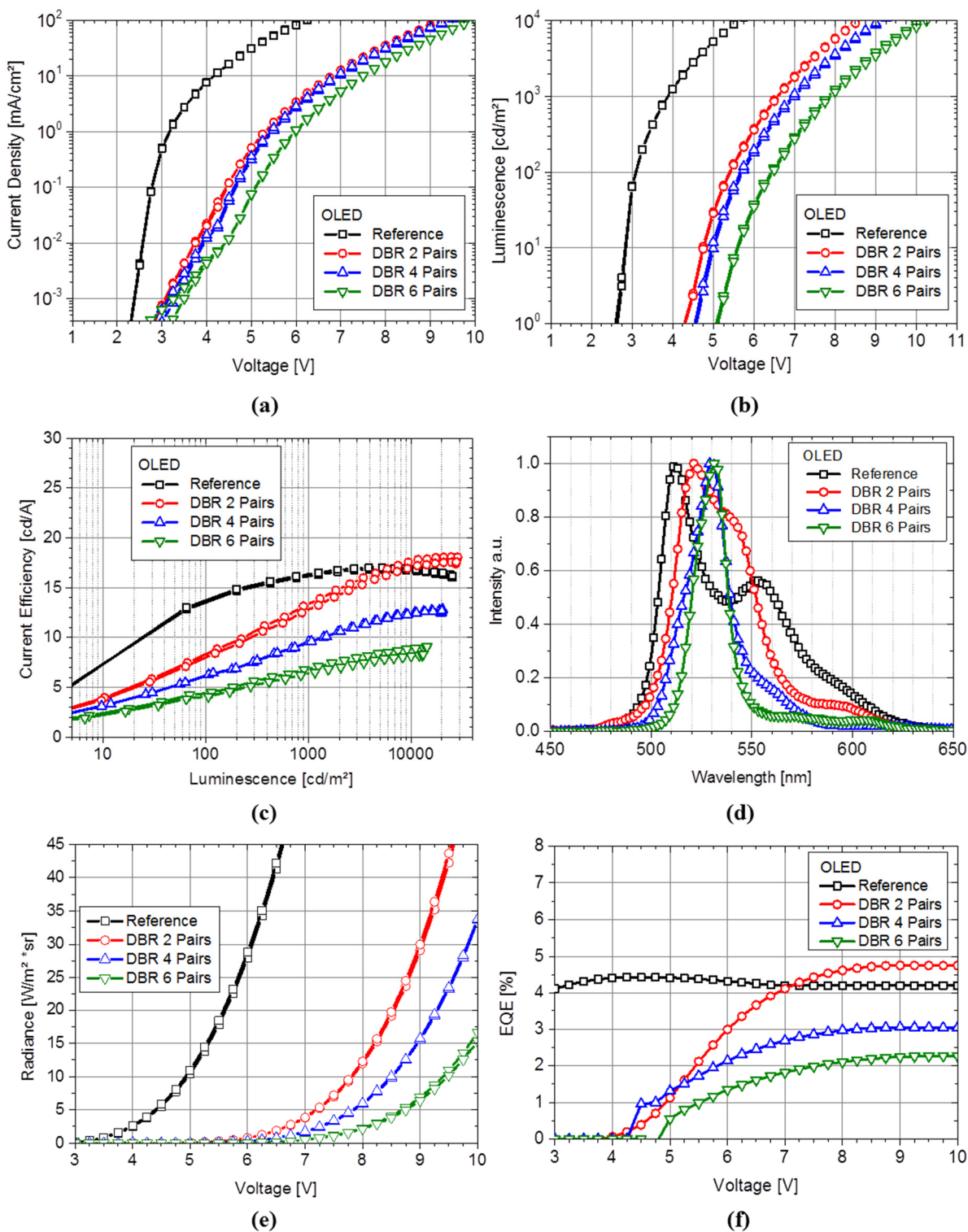


Figure 1. (a) Current density to voltage curve ($J-V$ curve) of all devices; (b) determined luminescence characteristic of the devices; (c) current efficacy vs. luminescence and (d) the emission spectra of the devices in variation of the mirror pair number measured perpendicular to the OLED surface. Figure (e) and (f) show the radiometric values: (e) the radiance depending on voltage and (f) the external quantum efficiency.

Figure 2 exhibits the cross section of the OLED devices with DBR mirrors. The sequence of the dielectric layers can be identified and does not show any interface defects between spacer layer and DBR

or any delamination of organic layers from the contacts. However, looking in more detail, we notice a discontinuity of our silver cathode at each device. We believe that this is not originating from a temperature effect or induced stress during the DBR deposition; moreover, it can be assigned to the typical thin film formation behavior of silver during deposition. Similar effects are also described in the work of Lee and Schubert *et al.* [27–29].

Since the main focus of our experiment is based on organic sensor technology and the narrowing of the OLED emission spectra to stimulate the R6G, we consider the imperfections of the silver layer as negligible. The reduction to a narrow emission spectra of the OLED at 530 nm wavelength is essential and a crucial point in this study. In Figure 1d, we present the resulting emission profile variation at a luminance of 1000 cd/m².

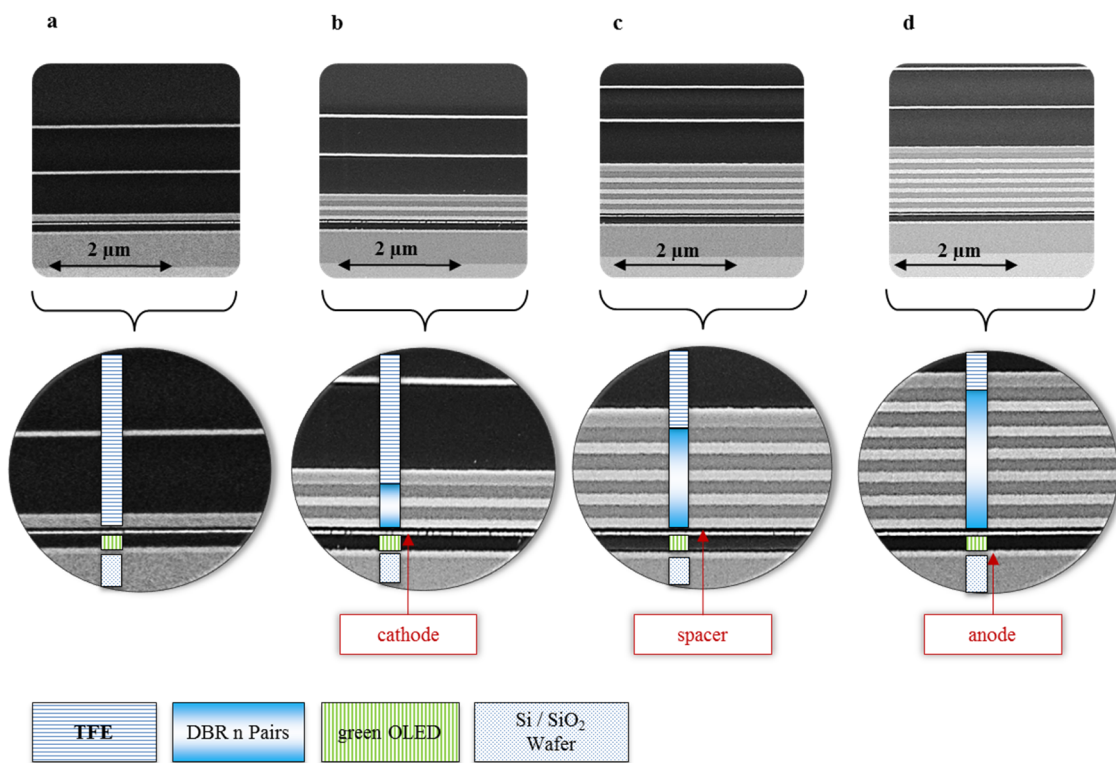


Figure 2. Cross section of the OLED devices including the variation of DBR layer and fixed TFE-thicknesses, (a) shows the reference OLED; (b) shows two pairs of DBR on top of OLED including TFE (2.0 kV/1.6 mm × 20.0 k); (c) shows four pairs of DBR (2.0 kV/1.8 mm × 20.0 k) and (d) exhibits six pairs of DBR above the OLED and below the TFE with (2.0 kV/2.3 mm × 20.0 k).

The emission spectrum for the reference device is located between 480 nm and 630 nm with a maximum at 510 nm. The DBR mirror uses the transmission with a defined stop band and acts as dielectric mirror. With increasing numbers of DBR pairs, the emission maxima shift towards 530 nm while also reducing the full width at half maximum (FWHM). Whereas the significance of emission maximum variation reduces with every additional DBR pair (510 nm with 0 pairs, 521 nm with two pairs, 530 nm with four and six pairs), the FWHM width decreases with each new pair (42 nm with two pairs, 24 nm with four pairs, 18 nm with six pairs). Figure 3a,b illustrate the emission spectra of individual OLEDs depending on mirror properties. To separate the excitation spectra from the emission

a sharp cut off at 550 nm for R6G is needed. In Figure 3a, the reference device without any mirror shows a significant overlap at 550 nm and a deviation in maximum of excitation. In contrast to the reference, the devices with DBR mirror exhibit a substantial improvement to stimulate the absorption of the pigment.

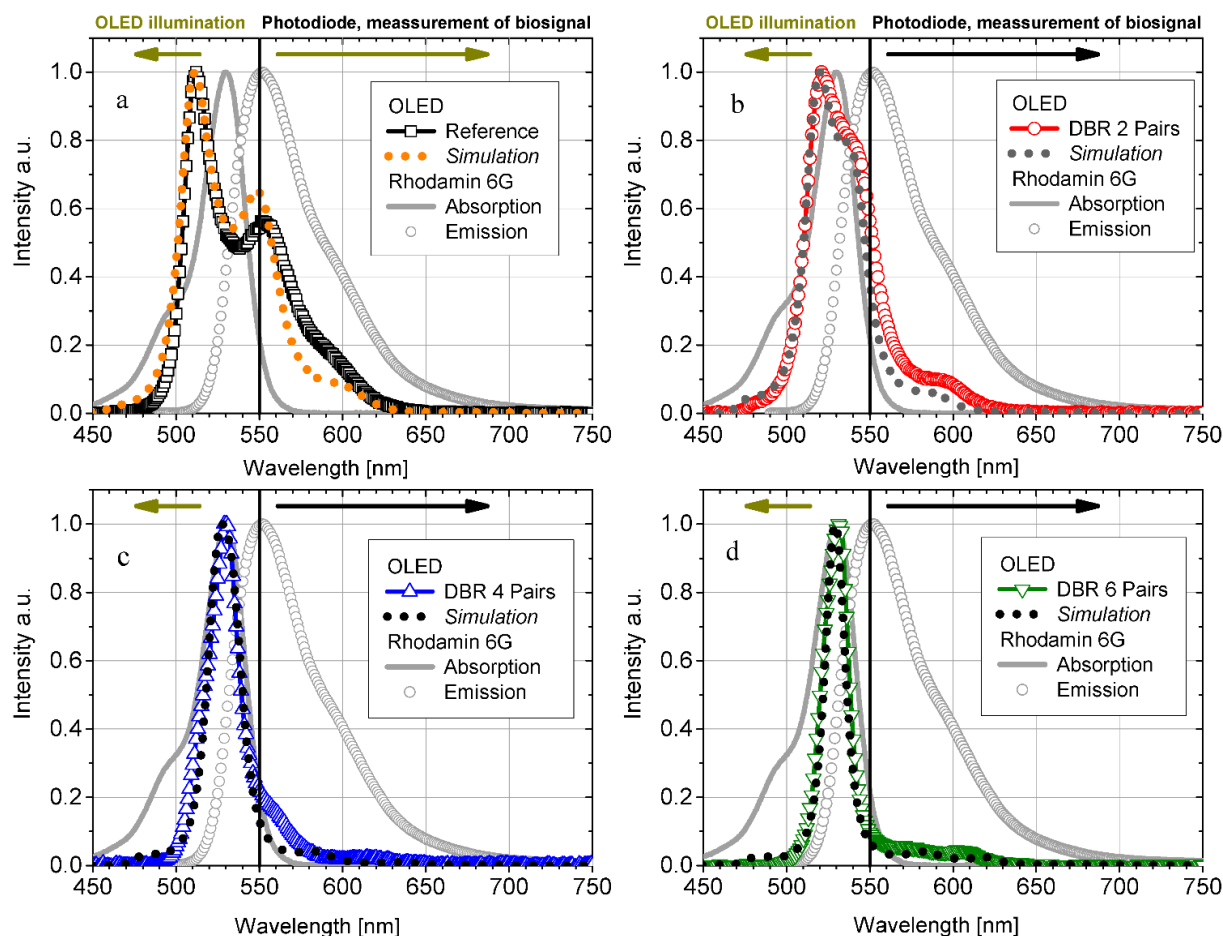


Figure 3. All graphs express the normalized spectral radiance as intensity. The graphs in (a) exhibit the spectral emission of the reference OLED in comparison to the OLED devices with including DBR mirror; (b) two DBR Pairs; (c) four DBR pairs; (d) six DBR pairs. The grey solid line presents the excitation spectra and the open dotted line the emission spectra of R6G in a water solution excited and recorded with a Fluoromax-4 from Horiba Jobin Yvon. Furthermore, the figures demonstrate the result of our experiment with the previous simulation.

As depicted in Figure 3b, we achieved a reduced overlap and a shift of the emission peak towards 530 nm for two DBR pairs. Consequently, Figure 3c,d reveal that devices comprising four and six DBR pairs are featured by the most suitable optical properties to excite the R6G in their excitation maximum at 530 nm. The maximum of emission is located at the required peak for both devices while the six pair DBR OLED shows a good cut-off at the wavelength of 550 nm. Therefore, the OLED device with six DBR pairs demonstrates the best result to stimulate the pigment R6G and to separate the emission of the excitator and analyte. For developments in sensor technology, it is important to understand the optical properties of materials and processes as well as their impact to the final device. For comparison, the experimental data are plotted together with the results from optical simulation of the OLED emission characteristic. Figure 3a–d illustrate the recorded, normalized spectra in comparison to the simulated

emission spectra. With respect to the reference OLED, we achieved a good correlation with the simulated and recorded spectra. The simulated data and experimental results differ slightly between 530 nm and 600 nm. However, this discrepancy can be attributed to differences in the modelling of the emission characteristic of less efficient recombination centers at the green emitter molecule and is not important for the spectral shape of the design of DBR mirror. Figure 3b–d present the experimental results and simulation data in variation of the mirror number. With increasing DBR pair number, the OLED emission characteristic is strongly modified with respect to the spectral shape as well as the FWHM, whereas the emission spectra are affected as simulated due to the increasing number of dielectric layers and the emission spectra are narrowed. This change in the emission spectrum originates from alternating thin dielectric layers of different refractive indices. Each dielectric and polymer layer boundary causes a partial reflection of an optical wave. In case the wavelength is close to four times the optical thickness of the DBR layers, the majority of reflections combine to constructive interference, and the layers act as an excellent reflector with the expected stop band at 530 nm. By comparing the measured OLED characteristics with simulation, we attribute the deviation of the optical cavity to the thickness of DBR layers, unclosed Ag cathode and a slight layer inhomogeneity in the thin film encapsulation. Optical simulations show the high sensitivity of DBR-OLED emission properties to thickness and material properties with increasing DBR thickness. Thus, the advantage of emission optimization is accompanied by an increase in requirements of multilayer deposition accuracy. Nevertheless, the variation by the number of dielectric layers as illustrated in our experiment and schematic in Figure 4, exhibits an alternative option to control the optical behavior of light emission for OLED devices. The possibility to modify the light emission behavior of OLEDs by using optical mirrors like DBR has been demonstrated and can be applied for sensing such as illuminating R6G.

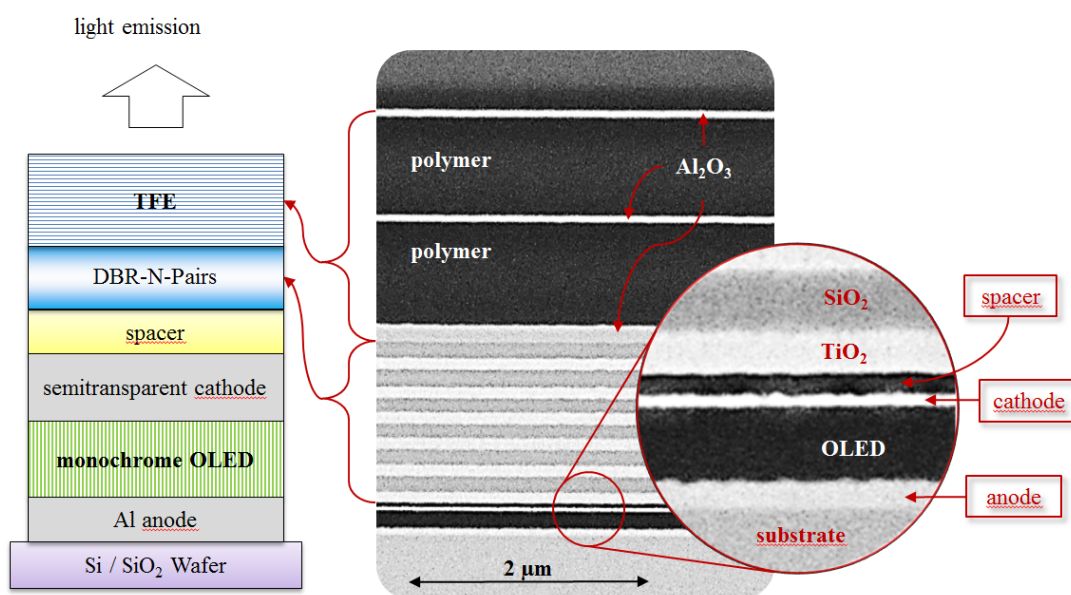


Figure 4. Schematic presentation of the device architecture including the top-emitting OLED, the DBR and the thin film encapsulation. N correlates to the number of DBR pairs ($N = 0, 2, 4, 6$).

3. Experimental Section

For OLED device preparation, an aluminum (Al) anode was deposited via sputtering onto a silicon oxide insulation layer on the silicon substrate. Subsequently, several organic layers of the monochrome OLEDs are deposited on top of the structured anode by vapor thermal evaporation (VTE) under a base pressure of 2×10^{-7} mbar. The total OLED thickness is 108 nm and comprises different functional layers such as the hole injection layer (HIL) and a hole transport layer (HTL). The HIL consists of 1,4,5,8,9,11-hexa-azatriphenylene hexacarbonitrile (HATCN; 10 nm) and the HTL of *N,N'*-bis(naphthalene-1-yl)-*N,N'*-bis(phenyl)-2,7-diamino-9,9-spirobifluorene (spiro-NPB; 50 nm). Both materials were delivered by Nichem Fine Technology Co. Ltd (NFT) (Jhubei City, Hsinchu County, Taiwan). The emission layer (20 nm) consisting of a host material and 5% dopant material and were provided from Sun Fine Chemical (Ochang-eup, Cheongwon-gun, Chungcheongbuk-do, South Korea). Furthermore an electron transport layer (ETL) (28 nm) is used. The ETL based on host material delivered by Merck KGaA (Darmstadt, Germany) and a 16.8% dopant of 8-hydroxyquinolatolithium (LiQ) provided by NFT. The OLED is completed with an electrical contact which consists of a transparent cathode (2 nm Ca, 13 nm Ag) provided by Kurt J. Lesker (Hastings, England). The cross section of cathode and anode films defines the active pixel area of 2.50×2.54 mm². The OLED is finalized by depositing an organic spacer layer (30 nm) spiro-NPB delivered by NFT to reduce the thermally induced stress of the subsequent optical mirror and its influence on the underlying cathode film. The individual lateral dimensions of each layer are defined by the used shadow masks. The optical mirror consists of alternating silicon dioxide (SiO₂) and titanium dioxide (TiO₂) layers, deposited via electronic-beam evaporation with a rate of 0.2 nm/s for SiO₂ and 0.1 nm/s for TiO₂. The SiO₂ and TiO₂ materials were purchased from Kurt J. Lesker company. The DBR features 95 nm thick SiO₂ and 64 nm thick TiO₂ layer pairs. (DBR with two pairs: 318 nm total thickness, four pairs: 636 nm total thickness and six pairs: 954 nm total thickness). Finally, a 1.3 μm thick multilayer thin-film encapsulation (TFE) is applied to protect the device against damage and degradation. This TFE consists of alternating layers of aluminum oxide (Al₂O₃) provided by Kurt J. Lesker and a cross-linked acrylic polymer from JSR Micro. The TFE is made of a 100 nm Al₂O₃ layer by electronic-beam evaporation and followed by direct current sputtering of 40 nm Al₂O₃ for two times. The polymer between the Al₂O₃ is produced by a liquid-vapor-liquid deposition and is cured with UV light. More details about this thin film encapsulation system are published elsewhere [30]. The adhesion of water within the DBR can also cause a shift of the photonic bandgap. Therefore, the TFE is used in addition to protect the optical design of the DBR. The Figure 4 illustrates the schematic cross section of the described device architectures, as confirmed by field emission scanning electron microscopy (FE-SEM) images, while, in Figure 5, the optical properties of the used DBR and TFE materials are shown. In addition, Figure 2 exhibits a detailed view on the layer structure of the OLED device. The whole process of device fabrication in combination with DBR and encapsulation has been performed in cleanroom environment of class ISO 5, while only the separation of OLED devices from each other and their characterization were done under laboratory conditions. After fabrication, the devices have been characterized by means of measuring current density-voltage (j - V), luminance-voltage (L - V) and the electroluminescent spectra in the range from 1 to 10 V. The OLED characterization is carried out with an Autronic Melchers System (DMS401). The preparation and analysis of the cross section in Figures 2 and 4 has been performed by a 6 kV argon ion beam (Jeol, Cross-Section Polisher SM-09010) with a

beam diameter full width at half maximum of 500 μm . The characterization of these cross sections was done with an FE-SEM (Hitachi SU8000) at an accelerating voltage of 2.0 kV and different resolutions. For two-pair DBR, we are using an operating distance of 1.6 mm with a magnification of 20000 and for four-pair DBR a distance of 1.8 mm and a magnification of 20,000 and finally for the six-pair DBR, a distance of work with 2.3 mm and the same magnification like four-pair DBR.

For optical simulation, we are using the emission module of the thin film optics simulation software “SETFOS”, version 3.3. SETFOS applies the transfer matrix approach to calculate the optical properties of a multilayer structure and the emission profile is derived by considering the complex refractive index and optical thickness of each layer, where n is the refractive index and k is the extinction coefficient and x describe the layer thickness. We extract the optical constants such as the refractive index and extinction coefficient for organic and metal films by analyzing recorded data obtained from variable-angle spectroscopic ellipsometry (M2000 Woollam) (VASE) with an analyzer (NIR-VIS-UV VASE, J.A. Woollam Co. Inc., Lincoln, USA). The modelling principle for OLEDs is described and published elsewhere [31,32].

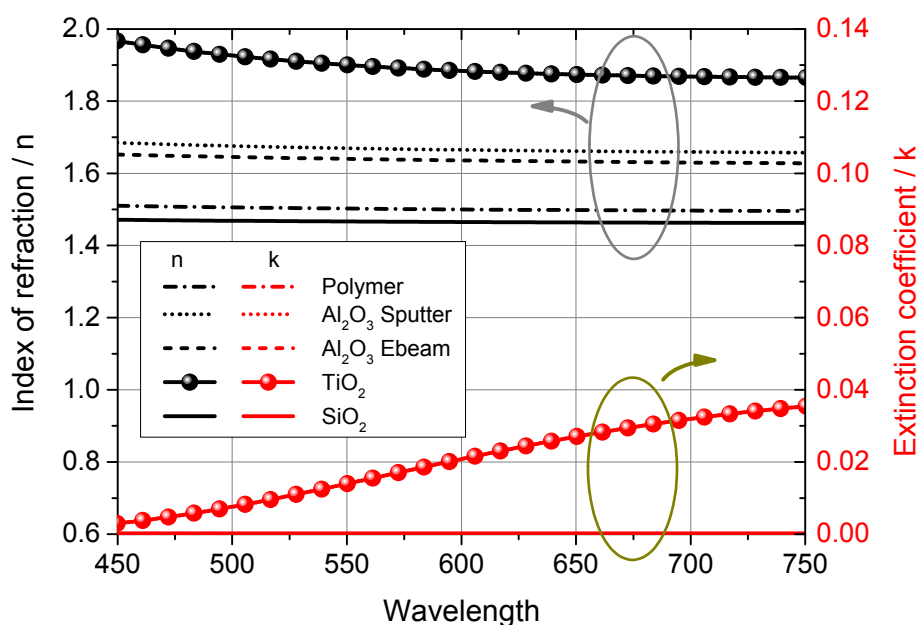


Figure 5. The optical constants n and k for the used DBR materials and the TFE.

4. Conclusions

In conclusion, we have proved the concept to use dielectric mirrors integrated in OLED devices for bio-chemical sensor applications. We investigated the opportunity to use DBR mirrors in combination with a thin-film encapsulation to illuminate designated excited states of R6G. The controlled excitation was realized by three different kind of DBR pairs on top of the OLED device and demonstrates the possibility to combine organic based devices with the technology of included optical mirrors. We designed the OLED to fulfil the excitation requirements of 530 nm as well as the sharp cut off above 550 nm. The change of light emission characteristics and cutoff wavelength was described by means of multilayer optics using SiO_2 and TiO_2 as DBR-materials. These findings enable the use of OLEDs emitting in the

ultraviolet, visible or near infrared region of light in biological sensors especially designed for reduced optical crosstalk.

Acknowledgments

We would like to thank Bolko Schöneich for fitting and calculating the optical constants and Denis Kaske and Carsten Schöberle as well as Thomas Sonnabend for their helpful support in the process. Olaf Zywitzki and Thomas Modes are acknowledged for the preparation of the devices for FE-SEM study. Additionally, we would like to thank the European Union with the project ADMONT and the Federal Ministry of Education and Research (BMBF) and Sächsische Aufbau Bank (SAB) for their financial support. The project ADMONT has received funding from the European Union's H2020 Programme (ECSEL) under grant agreement number 661796 besides the SAB and BMBF finance this work under grand agreement number 16ESE0058S.

Author Contributions

The conception and design was carried out by Matthias Jahnel and Michael Thomschke. In addition, the simulation of the mirror as well as the OLED was done by Matthias Jahnel. The data collection, analysis and interpretation was carried out by Matthias Jahnel and was revised by Beatrice Beyer and Michael Thomschke. Matthias Jahnel and Beatrice Beyer wrote the manuscript and Felix Kruczak revised the article from a relevant and biological point of view. The critical revision of the article was done by Karsten Fehse and Karl Leo.

Conflicts of Interest

The authors declare no conflict of interest.

References

1. Osgood, R.M., Jr.; Javan, R.; Sackett, P.B. Measurement of Vibration-Vibration Energy transfer time in HF gas. *Appl. Phys. Lett.* **1972**, *20*, 469–472.
2. Shinar, R.; Shinar, J. *Organic Electronics in Sensors and Biotechnology*, 1st ed.; McGraw-Hill Companies: New York, NY, USA, 2009; pp. 165–191.
3. Wang, J.H.; Bartlett, J.D.; Dunn, A.C.; Small, S.; Willis, S.L.; Driver, M.J.; Lewis, A.L. The use of rhodamine 6G and fluorescence microscopy in the evaluation of phospholipid-based polymeric biomaterials. *J. Microsc.* **2005**, *217*, 216–224.
4. Wang, Y.; Wang, J. Photoacoustic microscopy using Förster resonance energy transfer. *J. Biomed. Opt.* **2012**, *17*, 086007, doi:10.1117/2.1201211.004595.
5. Bujko, A.; Bojarski, C.; Bujko, R. Investigation of anti-Stokes fluorescence in mixed rhodamine 6G-Malachite green systems. *J. Acta Phys. Hungar.* **1983**, *54*, 139–146.
6. Jaworska, A.; Wojcik, T.; Malek, K.; Kwolek, U.; Kepczynski, M.; Ansary, A.A.; Chlopicki, S.; Baranska, M. Rhodamine 6G conjugated to gold nanoparticles as labels for both SERS and fluorescence studies on live endothelial cells. *Microchim. Acta* **2015**, *182*, 119–127.

7. Evans, T.; Brew, D.; Toole, K.; Colella, M.; Lennard, C.; Roux, C.; Walsh, S. Investigating the Impact of Radiation and Radioactive Contamination on Forensic Trace Evidence, ANSTO, 2012. Available online: <http://www.ansto.gov.au/AboutANSTO/MediaCentre/News/ACS012965> (accessed on 1 July 2015).
8. Peng, H.J.; Wong, M.; Kwok, H.S. Design and Characterization of Organic Light Emitting Diodes with Microcavity Structure. *SID Symp. Dig. Tech. Pap.* **2013**, *34*, 516–519.
9. Hwang, Y.; Lee, H.; Won, T. Optical characteristics of organic green-light-emitting devices: Finite element approach. *J. Appl. Phys.* **2014**, *53*, 08ND01.
10. Xiang, C.; Koo, W.; SO, F.; Sasabe, H.; Kido, J. A systematic study on efficiency enhancements in phosphorescent green, red and blue microcavity organic light emitting devices. *Nat. Light: Sci. Appl.* **2013**, *2*, e74, doi:10.1038/lssa.2013.30.
11. Jeong, S.M.; Takanishi, Y.; Ishikawa, K.; Takezoe, H. Flexible Microcavity Organic Light-Emitting Diodes with Wide-Band Organic Distributed Bragg Reflector. *Jpn. J. Appl. Phys.* **2006**, *45*, L73.
12. Zhang, H.; Chen, S.; Zhao, D. Surface-plasmon-enhanced microcavity organic light-emitting diodes. *Opt. Soc. Am.* **2014**, *22*, S7, doi:10.1364/OE.22.0A1776.
13. Brückner, R.; Lyssenko, V.G.; Hofmann, S.; Leo, K. Lasing of Tamm states in highly efficient organic devices based on small-molecule organic semiconductors. *RSC Faraday Discuss.* **2014** *174*, 183–201.
14. Chang, W.; Wang, A.; Murarka, A.; Akselrod, G.M.; Packard, C.; Lang, J.H.; Bulović, V. Electrically tunable organic vertical-cavity surface-emitting laser. *Appl. Phys. Lett.* **2014**, *105*, 073303, doi:10.1063/1.4893758.
15. Nicholson, R.A.; Li, G.H.; Buenaventura, E.; Graham, D. A rapid and sensitive assay for paralytic shellfish poison (PSP) toxins using mouse brain synaptoneurosomes. *Toxicon* **2002**, *6*, 831–838.
16. Baatz, H.; Steinbauer, M.; Harris, A.G.; Krombach, F. Kinetics of White Blood Cell Staining by Intravascular Administration of Rhodamine 6G. *Int. J. Microcirc. Clin. Exp.* **1995**, *15*, 85–91.
17. Ranjbari, E.; Hadjmohammadi, M.R. Optimization of magnetic stirring assisted dispersive liquid-liquid micro extraction of rhodamine B and rhodamine6G by response surface methodology: Application in water samples, soft drink, and cosmetic products. *Talanta* **2015**, *139*, 216–225.
18. Jamison, J.K.; Krabill, K.; Hatwalker, A.; Jaminson, E.; Tsai, C.C. Potentiation of the antiviral activity of poly r(A-U) by xanthene dyes. *Cell Biol. Inter. Rep.* **1990**, *14*, 1075–1084.
19. Kutushov, M.; Gorelik, O. Low concentrations of Rhodamine-6G selectively destroy tumor cells and improve survival of melanoma transplanted mice. *Neopl* **2013**, *60*, 262–273.
20. Fu, Y.; Jiang, X.J.; Zhu, Y.Y.; Zhou, B.J.; Zang, S.Q.; Tang, M.S.; Zhang, H.Y.; Mak, T.C.W. A new fluorescent probe for Al³⁺ based on rhodamine 6G and its application. *RSC Dalton Trans.* **2014**, *43*, 12624–12632.
21. Bokhale, N.B.; Bomble, S.D.; Dalbhanjan, R.R.; Mahale, D.D.; Hinge, S.P.; Banerjee, B.S.; Mohod, A.V.; Gogate, P. R. Sonocatalytic and sonophotocatalytic degradation of Rhodamine 6G containing wastewaters. *Ultrason. Sonochem.* **2014**, *21*, 1797–1804.
22. Ren, H.; Kulkarni, D.; Kodiyath, R.; Xu, W.; Choi, I.; Tsukruk, V.V. Competitive Adsorption of Dopamine and Rhodamine 6G on the Surface of Graphene Oxide. *ACS Appl. Mater. Interfaces* **2014**, *6*, 2459–2470.

23. Peng, H.; Sun, J.; Zhu, X.; Yu, X.; Wong, M.; Kwok, H.S. High-efficiency microcavity top-emitting organic light-emitting diodes using silver Anode. *Appl. Phys. Lett.* **2006**, *88*, 073517, doi:10.1063/1.2172734.
24. Zhou, H.; Park, J.W. The effects of compressive stress on the performance of organic light-emitting diodes. *Org. Electron.* **2015**, *24*, 272–279.
25. Cester, A.; Bari, D.; Framarin, J.; Wrachien, N.; Meneghesso, G.; Xia, S.; Adamovich, V.; Brown, J.J. Thermal and electrical stress effects of electrical and optical characteristics of Alq3/NPD OLED. *Microelectron. Reliab.* **2010**, *50*, 1866–1870.
26. Zhao, Y.; Chen, J.; Ma, D. Ultrathin Nondoped Emissive Layers for Efficient and Simple Monochrome and White Organic Light-Emitting Diodes. *ACS Appl. Mat. Interfaces* **2013**, *5*, 965–971
27. Lee, C.; Robertson, C.S.; Nguyen, A.H.; Kahramanz, M.; Wachsmann, H.S. Thickness of a metallic film, in addition to its roughness, plays a significant role in SERS activity. *Nat. Sci. Rep.* **2015**, *5*, 11644, doi:10.1038/srep11644.
28. Schubert, S.; Hermenau, M.; Meiss, J.; Müller-Meskamp, L.; Leo, K. Oxide Sandwiched Metal Thin-Film Electrodes for Long-Term Stable Organic Solar Cells. *Adv. Funct. Mater.* **2012**, *22*, 4993–4999
29. Schubert, S.; Meiss, J.; Müller-Meskamp, L.; Leo, K. Improvement of Transparent Metal Top Electrodes for Organic Solar Cells by Introducing a High Surface Energy Seed Layer. *Adv. Energy Mater.* **2013**, *3*, 438–443.
30. Park, J.S.; Chae, H.; Chung, H.K.; Lee, S.I. Thin film encapsulation for flexible AM-OLED: A review. *IOP-Sci. Semicond. Sci. Technol.* **2011**, *26*, 3.
31. Ruhstaller, B.; Beierlein, T.; Riel, H.; Karg, S.; Scott, J.C.; Riess, W. Simulating Electronic and Optical Processes in Multilayer Organic Light-Emitting Devices. *IEEE J. Sel. Top. Quantum.* **2008**, *9*, 723–731.
32. Riel, H.; Karg, S.; Beierlein, T.; Riess, W.; Neyts, K. Tuning the emission characteristics of top-emitting organic light-emitting devices by means of a dielectric capping layer: An experimental and theoretical study. *J. Appl. Phys.* **2003**, *94*, 5290–5296.